IEEE Access
Multidisciplinary | Rapid Review | Open Access Journal

Received April 9, 2018, accepted May 22, 2018, date of publication May 30, 2018, date of current version December 31, 2018.

Digital Object Identifier 10.1109/ACCESS.2018.2842079

Dual Function System With Shared Spectrum Using FMCW

CHAO YANG[1], MEI WANG[1,2], LIN ZHENG[1,3], AND CHAOCHEN TANG[2]

[1]Provincial Ministry of Education Key Laboratory of Cognitive Radio and Signal Processing, Guilin University of Electronic Technology, Guilin 541004, China
[2]Institution of Information Science and Engineering, Guilin University of Technology, Guilin 541004, China
[3]Science and Technology on Communication Networks Laboratory, Guilin University of Electronic Technology, Shijiazhuang 050081, China

Corresponding author: Mei Wang (mwang@glut.edu.cn)

This work was supported in part by the National Natural Science Foundation of China under Grant 61771151 and Grant 61071088, in part by the Guangxi Key Laboratory of Wireless Wideband Communication and Signal Processing under Project GXKL061501, and in part by the Science and Technology on Communication Networks Laboratory under Project KX172600033.

ABSTRACT Although an automotive radar system tends to be practical presently, it still needs to set up an extra device to achieve communication for vehicle. Considering system complexity and equipment costs, the research on automotive radar and communication integration has a very good application prospect. These days, there has been some research work on radar and communication integration based on the traditional LFMCW, but not involving triangle LFMCW, FSK, and MFSK waveform used typically for automotive radar, and its realization of dual function mainly depends on frequency diversity, meaning that systems need to occupy more spectrum resources. In this paper, a method on radar and communication integration with shared spectrum is proposed by using FMCW, which combines between Chirp-BOK modulation and FSK radar. In the system, communication information can be demodulated by decision on chirp polar, and target information can be extracted from phases of chirp. Moreover, to reduce the complexity of the receiver, a matching filter method is used commonly to complete the implementation of dual function in the system. However, it is necessary to note that the Doppler effect make phases of matching output change, which has an impact on target detection based on FSK. Therefore, the relationship of phases between Doppler and matching output will be analyzed first. Then, the system's operating principle, derivation of the algorithm, the limitation of system parameters selection, and simulation results are described in this paper.

INDEX TERMS Automotive application, FMCW radar, Chirp-BOK, Radar and communication integration.

I. INTRODUCTION

Along with the rising of the people's safe consciousness, the concept of intelligent transportation has taken this to their hearts. Its core technologies are Vehicle Collision System (VCS) and Vehicle-to-Vehicle communication (V2V), which are based on a radar system and a communication system, respectively. On the one hand, such a dual system architecture increases both the complexity and the cost of the vehicle system. Moreover, the dual system need occupy spectrum resource at the different frequency bands, which undoubtedly increases the load of spectrum resources in the current era of the lack. On the other hand, the design of radar-communication integration has become the future development tendency, so it is valuable to combine VCS and V2V into a system.

Several studies on automotive radars using FMCW are reported. The earliest anti-collision radar is based on LFMCW, which can obtain high distance and velocity resolution by the way of dechirp, but existing the couple of distance and velocity [1]. Symmetrical triangle LFMCW waveform is proposed to solve the couple problem, but ghost targets may occur in multi-target environment [2]. Triangle LFMCW with different modulate frequency slope can get the same location for real targets, but is different for ghost targets. Based on this idea, multi-slope triangle LFMCW waveform is proposed [3], [4], whose drawbacks are disparity of symbol length or bandwidth for each triangle waveform, and a long measurement time is needed which is a contradiction to a high update rate. So another option is FSK radar based on the idea of phase difference generated by different frequency signals for a target. It can only use phase changes between different symbols to obtain target's range and velocity, but cannot distinguish multi-targets with the same velocity. To further acquire unambiguous range and velocity measurement with

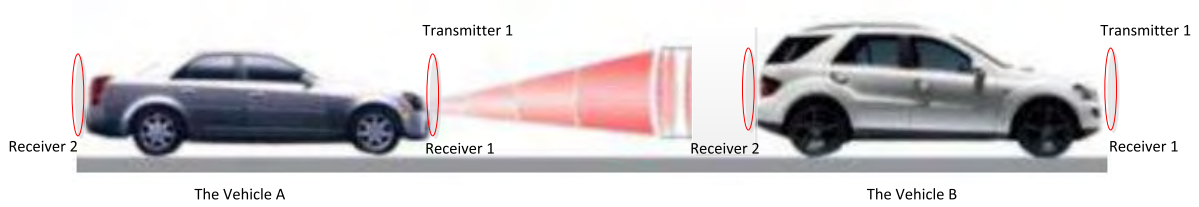

FIGURE 1. Scenario diagrams of vehicle system integrated radar and communication.

high resolution and accuracy in multi-targets situation, two waveforms combined between LFMCW and FSK are proposed by Hermann Rohling. One is using two chirp signals with different initial frequency [6], and the other is using two intertwined stepped frequency signals with different initial frequency [5], called as MFSK. Above algorithms only solve detection problem for targets, but not considering how to embed communication information into radar signal.

Actually, radar and communication integration based on LFMCW signal has been studied in the early 2000s. Some scholars discovered that up-chirp and down-chirp at adjacent frequency bands maintain orthogonality at some degree, and the overlap part of both can reach 25% of its own bandwidth in 2001 [7]. So some researchers attempt to load radar and communication function into two chirp signals with opposite slope, respectively [8]–[10]. Afterward, P Barrenechea et al. proposed a combination of amplitude modulation and FMCW radar in 2007, called as AM-FMCW [11]. Soon after, Werner Scheiblhofer et al. replaced amplitude modulation with FSK modulation and combined with FMCW radar in 2015 [12]. The common above these methods have is that the frequency bands occupied for radar and communication systems are different, in other words, dual functions are achieved by spectrum diversity. Furthermore, above researches on radar and communication mainly focus on traditional LFMCW radar, not involving triangle LFMCW, FSK and MFSK waveform used typically for automotive radar.

In this paper, a scenario diagram of vehicle system with communication and radar function is shown as Fig.1. In this scenario, transmitter 1 of vehicle A can send communication messages to receiver 2 of vehicle B, and vehicle B can get velocity and distance to the back vehicle A from direct signal of A to B. On the other hand, vehicle A need also get velocity and distance to the front vehicle B from echo reflected from vehicle B. For all this, a method on radar and communication integration with shared spectrum is proposed by using FMCW, which loads Chirp-BOK modulation into FSK radar by constructing two Chirp-BOK channels with different initial frequency, called as CFSK in this paper. Its inspiration comes from demodulation for Chirp-BOK, which only use the amplitude of matching output but the use of its phase is free. Moreover, FSK radar can only utilize phases to achieve range and velocity for targets. Besides, up-chirp and down-chirp have the same characteristic of matching output, providing favorable condition for coherent integration. Therefore, CFSK can achieve dual function by using information on amplitude and phase of matching output in the same frequency band. However, it's worth noting that even the envelope of matching output of Chirp is insensitive to doppler, but its phase is still affected by doppler. For this, the impact of doppler frequency on the phase of matching output of Chirp will be analyzed in section 2. The details about CFSK signal processing will be described in section 3, and the relation between system parameter setting and applicative condition is given in section 4. Finally, Simulation results will confirm the feasibility and validity of this proposed method in section 5.

II. MATCHING OUTPUT OF CHIRP WITH DOPPLER FREQUENCY

In this section, we will firstly analyze the doppler frequency effect on amplitude and phase of matching output of Chirp for use on subsequent sections. Generally, a baseband Chirp with doppler frequency is expressed as

$$s(t) = \begin{cases} A\exp\left[j2\pi\left(f_d t + \frac{1}{2}kt^2\right)\right], & |t| \le T_p/2 \\ 0, & else \end{cases} \quad (1)$$

where k, T_p, A, f_d are chirp-rate, symbol length, the amplitude of signal and doppler frequency, respectively. According to the Chirp's ambiguity function [13], its matching output can be expressed as

$$y_{doppler}(t) = A^2 T_p\left(1-\frac{|t|}{T_p}\right)\sin c\left[\pi\beta\left(\frac{f_d}{k}+t\right)\left(1-\frac{|t|}{T_p}\right)\right] \times \exp(j\pi f_d t) \quad |t| \le T_p/2 \quad (2)$$

Actually, transmitter just can produce a signal of $0 \le t \le T_p$ instead of $|t| \le T_p/2$, which lead to add an extra constant phase effected by doppler. Here, we provide a simple proof procedure based on matching on frequency domain. For a chirp of $0 \le t \le T_p$, its baseband signal should be expressed as

$$s(t) = \begin{cases} A\exp\left[j2\pi\left(-\frac{B}{2}t + f_d t + \frac{1}{2}kt^2\right)\right] & 0 \le t \le T_p \\ 0 & else \end{cases} \quad (3)$$

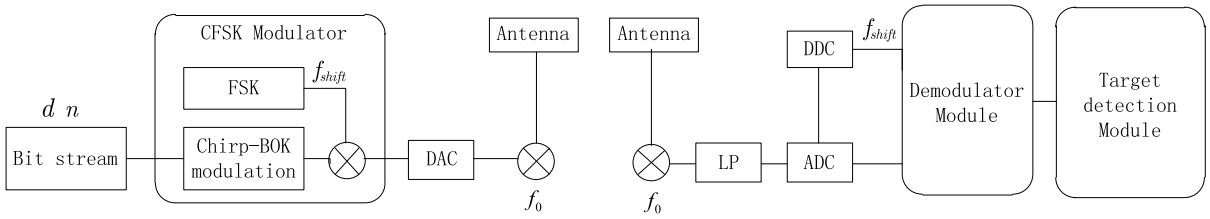

FIGURE 2. Block diagram of proposed CFSK system.

when time-bandwidth product $D \gg 1$, its corresponding frequency spectrum is approximated as

$$X(f) \approx \begin{cases} \frac{A}{\sqrt{k}} \exp\left\{j\left[-\pi (f-f_d)^2/k + \frac{\pi}{4}\right]\right\} \\ \quad \times \exp\left(-j\pi (f-f_d) T_p\right) \quad |f-f_d| \le \frac{B}{2} \\ 0 \qquad\qquad\qquad\qquad else \end{cases} \tag{4}$$

and frequency spectrum of matching filter on chirp is

$$H(f) = \begin{cases} \frac{A}{\sqrt{k}} \exp\left\{-j\left[-\pi f^2/k + \frac{\pi}{4}\right]\right\} \exp\left(j\pi f T_p\right) \\ \quad |f| \le \frac{B}{2} \\ 0 \quad else \end{cases} \tag{5}$$

So the matching output in frequency domain is

$$\begin{aligned} Y(f) &= X(f) H(f) \\ &= \frac{A^2}{k} \exp\left\{j\left[-\pi\left(f_d^2 - 2f_d f\right)/k\right]\right\} \exp\left(j\pi f_d T_p\right) \\ &= \frac{A^2}{k} \exp\left[j\left(-\pi f_d^2/k\right)\right] \exp[j(2\pi f_d f/k)] \exp(j\pi f_d T_p) \end{aligned} \tag{6}$$

where

$$\left|f - \frac{f_d}{2}\right| \le \frac{B}{2} - \frac{f_d}{2}$$

According to the inverse Fourier transform of gate function and the properties of IDFT, and let $B' = B - f_d$, its matching output in time domain is

$$\begin{aligned} s_{matching\_output}(t) = A^2 \frac{B'}{k} \sin c\left[\pi B'\left(t + \frac{f_d}{k}\right)\right] \\ \cdot \exp\left(j2\pi \frac{f_d}{2} t\right) \exp\left(j\pi f_d T_p\right) \end{aligned} \tag{7}$$

Compare to equation (2), it is more obvious to see that doppler frequency has impact on the envelope of matching output leading to the attenuation of amplitude, the increase of the main-lobe width. Moreover, an extra constant term associated with frequency f_d are introduced so that phase at peak is not zero but $P_{peak} = \pi f_d T_p - \pi f_d^2/k \approx \pi f_d T_p$ if $f_d \ll B$. This point requires particular attention if phase of chirp is used.

III. DUAL FUNCTION SYSTEM

A. CFSK SIGNAL MODEL

The block diagram of proposed CFSK system is illustrated in Fig. 2. To obtain CFSK signals, binary data $d[n] = 1$ *or* 0 is firstly passed through Chirp-BOK modulation with symbol interval T_p, then it is multiplied by FSK with a frequency offset f_{shift}. Here, we assume that even symbol is one without frequency offset and odd symbol is one with frequency offset. So the mathematic expression of CFSK transmitted with N symbols is given by

$$\begin{aligned} s(t) = \sum_{i=0}^{N-1} u_i\left(t - iT_p\right) \\ \cdot \exp\left[j2\pi\left(f_0 + \frac{1 + (-1)^{i+1}}{2} f_{shift}\right)\left(t - iT_p\right)\right] \end{aligned} \tag{8}$$

where t is sampling time, f_0 is the RF carrier frequency, and $u_i(t)$ is the baseband chirp signal of bandwidth B and chirp-rate k for ith symbol, can be expressed as

$$\begin{aligned} u_i(t) = \frac{1}{\sqrt{T_p}} rect\left(\frac{t - T_p/2}{T_p}\right) \\ \times \exp\left[j\left(-\pi Bt + \pi k t^2\right) c(i+1)\right] \end{aligned}$$

and

$$rect(t) = \begin{cases} 1 & |t| \le \frac{1}{2} \\ 0 & else \end{cases}$$

In addition, $c[n]$ is mapping from binary data $d[n]$, whose relation with $c[n]$ is $c(i+1) = 2d(i+1) - 1$. Here, Fig. 3 shows the relationship between the time- frequency diagram and data stream of transmitted signal.

Then transmitted CFSK signal will be sent to receiver 2 of vehicle B, and echo signal reflected from vehicle B will go back to receiver 1 of vehicle A, as shown below.

Suppose that the distance between A and B is R_0, and velocity of vehicle B is v relative to vehicle A, so

The delay of signal transmitted to receiver 1:

$$\tau_1 = 2(R_0 - vt)/c$$

The delay of signal reflected from receiver 2:

$$\tau_2 = (R_0 - vt)/c$$

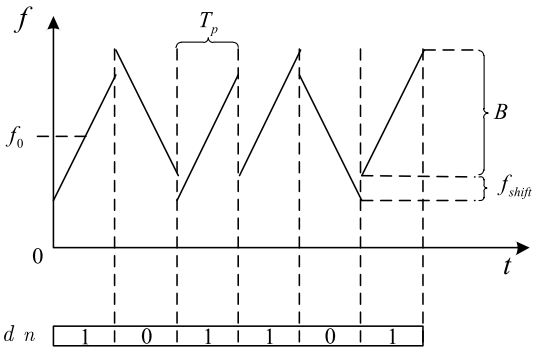

FIGURE 3. The time-frequency diagrams of transmitted signal.

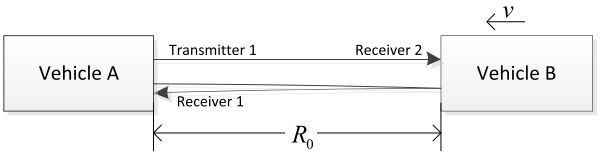

FIGURE 4. The channel propagation model.

So the both of received signal can be expressed as

$$r_1(t) = s(t - \tau_1) \tag{9}$$
$$r_2(t) = s(t - \tau_2) \tag{10}$$

Viewed from signal models in both receivers, its difference is just a factor of twice delay. So signal model can also take equation (9) as an example in subsequent sections, and the both signal processing steps can be the same, as shown in Fig.5. But it needs to note that the reference time point for target detection turns to be moment of frame synchronization instead of initial time of signal transmitted. Following signal processing is divided into two parts: the first one is demodulation module and the second one is target detection module.

B. DEMODULATION MODULE

There are two mixing channels of frequency $f_1 = f_0$ and $f_2 = f_0 + f_{shift}$ with the same initial phase ϕ_0 for down conversion, as seen from Fig.5. Its expression is

$$S_{1\_ref}(t) = \exp(j2\pi f_1 t + \phi_0) \tag{11}$$
$$S_{2\_ref}(t) = \exp(j2\pi f_2 t + \phi_0) \tag{12}$$

After echo signal is passed by two mixers, both baseband signal of expression of amplitude normalized are

$$\begin{aligned} S_{1\_base}(t) &= r(t)\exp[j(2\pi f_1 t + \phi_0)]^* \\ &= \sum_{i=0}^{N-1} u_i\left(t - iT_p - \tau\right) \\ &\quad \cdot \exp\left[j2\pi\left(\frac{1+(-1)^{i+1}}{2} f_{shift}\right)\left(t - iT_p - \tau\right)\right] \\ &\quad \cdot \exp\left\{j\left[2\pi f_1\left(-iT_p - \tau\right) - \phi_0\right]\right\} \end{aligned} \tag{13}$$

$$\begin{aligned} S_{2\_base}(t) &= r(t)\exp[j(2\pi f_2 t + \phi_0)]^* \\ &= \sum_{i=0}^{N-1} u_i\left(t - iT_p - \tau\right) \\ &\quad \cdot \exp\left[j2\pi\left(\frac{-1+(-1)^{i+1}}{2} f_{shift}\right)\left(t - iT_p - \tau\right)\right] \\ &\quad \cdot \exp\left\{j\left[2\pi f_2\left(-iT_p - \tau\right) - \phi_0\right]\right\} \end{aligned} \tag{14}$$

After chirp frame synchronization, sampling time for$i$symbol can be denoted as $t = t' + iT_p + 2R/c$, $t' \in [0, T_p - T_s]$, where t' is fast sampling time in a symbol. And the time delay generated by target can be represented as [14]

$$\begin{aligned} \tau &= 2\left[R - v\left(t' + iT_p + 2R/c\right)\right]/c \\ &= \frac{2R}{c} - \frac{2v}{c}t' - \frac{2v}{c}iT_p - \frac{2v}{c}\frac{2R}{c} \end{aligned}$$

So equation (13) and (14) turn into

$$\begin{aligned} &S_{1\_base}(t',\ i) \\ &= u_i\left[\left(1+\frac{2v}{c}\right)t' + \frac{2v}{c}iT_p + \frac{2v}{c}\frac{2R}{c}\right]\exp(-j\phi_0) \\ &\quad \cdot \exp\left\{j2\pi\left(\frac{1+(-1)^{i+1}}{2} f_{shift}\right)\right. \\ &\qquad \left.\times\left[\left(1+\frac{2v}{c}\right)t' + \frac{2v}{c}iT_p + \frac{2v}{c}\frac{2R}{c}\right]\right\} \\ &\quad \cdot \exp\left[j2\pi f_1\left(-iT_p - \frac{2R}{c} + \frac{2v}{c}t' + \frac{2v}{c}iT_p + \frac{2v}{c}\frac{2R}{c}\right)\right] \end{aligned} \tag{15}$$

$$\begin{aligned} &S_{2\_base}(t',\ i) \\ &= u_i\left[\left(1+\frac{2v}{c}\right)t' + \frac{2v}{c}iT_p + \frac{2v}{c}\frac{2R}{c}\right]\exp(-j\phi_0) \\ &\quad \times \exp\left\{j2\pi\left(\frac{-1+(-1)^{i+1}}{2} f_{shift}\right)\right. \\ &\qquad \left.\times\left[\left(1+\frac{2v}{c}\right)t' + \frac{2v}{c}iT_p + \frac{2v}{c}\frac{2R}{c}\right]\right\} \\ &\quad \cdot \exp\left[j2\pi f_2\left(-iT_p - \frac{2R}{c} + \frac{2v}{c}t' + \frac{2v}{c}iT_p + \frac{2v}{c}\frac{2R}{c}\right)\right] \end{aligned} \tag{16}$$

Then even and odd symbol can be extracted from channel 1 and channel 2, respectively. And its results are as following Let $i = 2n$, $n = 0, 1, 2\cdots\frac{N}{2} - 1$ in equation (13) for even symbol, thus

$$\begin{aligned} &S_{1\_base\_even}(t',\ 2n) \\ &= u_i\left[\left(1+\frac{2v}{c}\right)t' + \frac{2v}{c}2nT_p + \frac{2v}{c}\frac{2R}{c}\right]\cdot\exp \\ &\quad \times\left\{j\left[2\pi f_1\left(-2nT_p - \frac{2R}{c} + \frac{2v}{c}t' + \frac{2v}{c}2nT_p + \frac{2v}{c}\frac{2R}{c}\right)\right.\right. \\ &\qquad \left.\left.-\phi_0\right]\right\} \end{aligned} \tag{17}$$

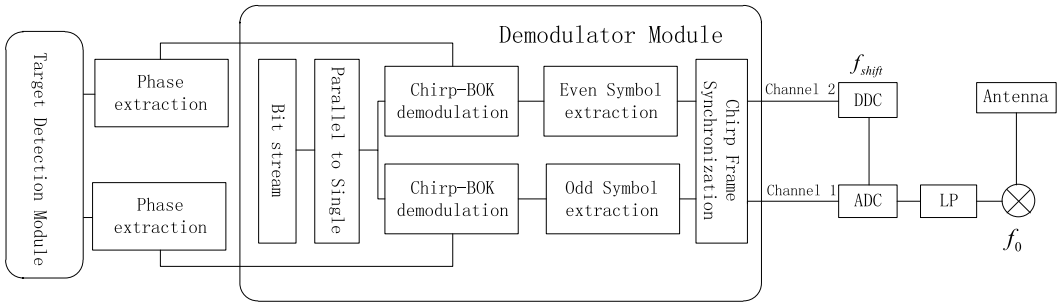

FIGURE 5. Block diagram of demodulation module.

Let $i = 2n+1, n = 0, 1, 2\cdots\frac{N}{2}-1$ in equation (14) for odd symbol, thus

$$\begin{aligned} &S_{2\_base\_odd}\left(t',\ 2n+1\right) \\ &= u_i\left[\left(1+\frac{2v}{c}\right)t' + \frac{2v}{c}\left(2n+1\right)T_p + \frac{2v}{c}\frac{2R}{c}\right] \\ &\cdot \exp\left\{j2\pi f_2\left[-\left(2n+1\right)T_p - \frac{2R}{c} + \frac{2v}{c}t'\right.\right. \\ &\left.\left. + \frac{2v}{c}\left(2n+1\right)T_p + \frac{2v}{c}\frac{2R}{c}\right] - j\phi_0\right\} \end{aligned} \tag{18}$$

Afterward, baseband chirp enters Chirp-BOK demodulation, its symbol decision is based on matching filter output of up-chirp and down-chirp. So to further analyze the impact on demodulation from target motion, we give the following four cases about matching filter output of up-chirp and down-chirp in both channels

$$\text{Denote: } f_d = \frac{2v}{c}f_1 \text{ and } f_{d2} = \frac{2v}{c}f_2$$

Case 1: when data is 1 for $S_{1\_base\_even}\left(t',\ 2n\right)$, according to the derivation in section II and considering $v \ll c$, the matching filter output towards up-chirp can be simplified as

$$\begin{aligned} &s_{match\_up}\left(t', 2n\right) \\ &\approx \frac{\sin\left[\pi B'\left(t' + \frac{f_d}{k} + \frac{2v}{c}2nT_p + \frac{2v}{c}\frac{2R}{c}\right)\right]}{\pi B'\left(t' + \frac{f_d}{k} + \frac{2v}{c}2nT_p + \frac{2v}{c}\frac{2R}{c}\right)} \\ &\times \exp\left[j2\pi f_d\left(t' + \frac{f_d}{k} + \frac{2v}{c}2nT_p + \frac{2v}{c}\frac{2R}{c}\right)\right] \\ &\times \exp\left(j2\pi\frac{2v}{c}f_1 2nT_p\right) \\ &\times \exp\left(-j2\pi f_1\frac{2R}{c}\right)\exp\left(j2\pi\frac{T_p}{2}f_d\right)\exp\left(j2\pi f_d\frac{2R}{c}\right) \\ &\times \exp\left[j2\pi f_1\left(-2nT_p\right)\right]\exp\left(-j\phi_0\right) \end{aligned} \tag{19}$$

Note that the magnitude is used for symbol decision but not utilizing its phase, so we need only focus on their envelope

$$\begin{aligned} &\left|s_{match\_up}\left(t', 2n\right)\right| \\ &= \left|\frac{\sin\left[\pi B'\left(t' + \frac{f_d}{k} + \frac{2v}{c}2nT_p + \frac{2v}{c}\frac{2R}{c}\right)\right]}{\pi B'\left(t' + \frac{f_d}{k} + \frac{2v}{c}2nT_p + \frac{2v}{c}\frac{2R}{c}\right)}\right| \end{aligned} \tag{20}$$

Case 2: when data is 0 for $S_{1\_base\_even}\left(t',\ 2n\right)$, the matching filter output towards down-chirp is

$$\begin{aligned} &\left|s_{match\_down}\left(t', 2n\right)\right| \\ &= \left|\frac{\sin\left[\pi B'\left(t' - \frac{f_d}{k} + \frac{2v}{c}2nT_p + \frac{2v}{c}\frac{2R}{c}\right)\right]}{\pi B'\left(t' - \frac{f_d}{k} + \frac{2v}{c}2nT_p + \frac{2v}{c}\frac{2R}{c}\right)}\right| \end{aligned} \tag{21}$$

Case 3: when data is 1 for $S_{2\_base\_odd}\left(t',\ 2n+1\right)$, the matching filter output towards up-chirp is

$$\begin{aligned} &\left|s_{match\_up}\left(t', 2n+1\right)\right| \\ &= \left|\frac{\sin\left\{\pi B'\left[t' + \frac{f_{d2}}{k} + \frac{2v}{c}\left(2n+1\right)T_p + \frac{2v}{c}\frac{2R}{c}\right]\right\}}{\pi B'\left[t' + \frac{f_{d2}}{k} + \frac{2v}{c}\left(2n+1\right)T_p + \frac{2v}{c}\frac{2R}{c}\right]}\right| \end{aligned} \tag{22}$$

Case 4: when data is 0 for $S_{2\_base\_odd}\left(t',\ 2n+1\right)$, the matching filter output towards down-chirp is

$$\begin{aligned} &\left|s_{match\_down}\left(t', 2n+1\right)\right| \\ &= \left|\frac{\sin\left\{\pi B'\left[t' + \frac{f_{d2}}{k} + \frac{2v}{c}\left(2n+1\right)T_p + \frac{2v}{c}\frac{2R}{c}\right]\right\}}{\pi B'\left[t' + \frac{f_{d2}}{k} + \frac{2v}{c}\left(2n+1\right)T_p + \frac{2v}{c}\frac{2R}{c}\right]}\right| \end{aligned} \tag{23}$$

Seen from case 1 to 4, the location at peak is walking with velocity of target, so the symbol synchronization will be affected due to adopt peak detection for chirp-BOK demodulation. Among them, the terms of range coupling shift caused by velocity for matching output is $\pm f_d/k$ and $\pm f_{d2}/k$, indicates that different polar chirp-rate signal produces moving at different directions, and the value of movement for different frequency carriers is not the same. On the other hand, the terms of peak walking caused by target motion for the period of multiple symbols is $2nT_p 2v/c$ and $(2n+1)\,T_p 2v/c$. Besides, $4vR/c^2$ is a constant range shift term. These factors will impact on symbol decision and phase extracted from peak, but $4vR/c^2$ can be generally neglected due to $v \ll c$,

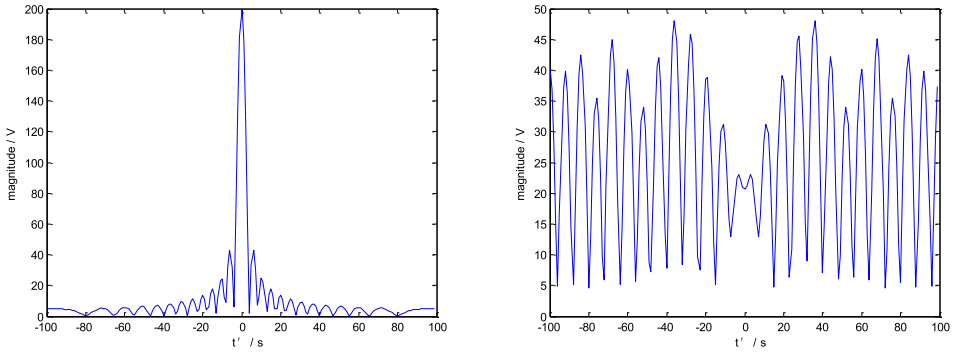

FIGURE 6. Comparison between up-chirp and down-chirp on the magnitude of matching filter output. (a) matching filter output between up-chirp and down-chirp. (b) matching filter output between up-chirp and up-chirp.

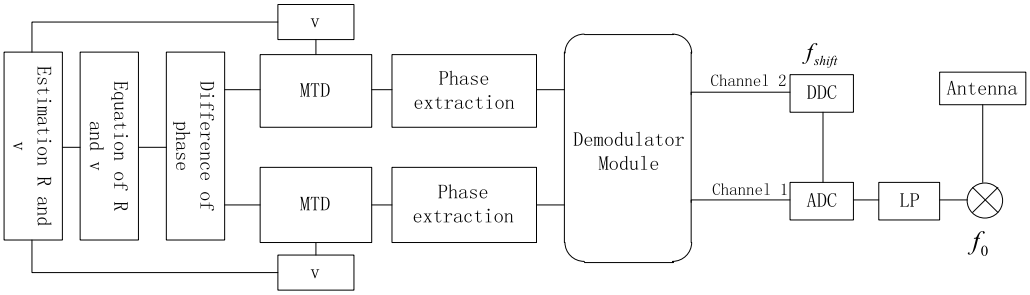

FIGURE 7. Block diagram of target detection module.

and others can be tolerated if it satisfies that peak shift is less than a width of mainlobe $1/B$, that meeting the following conditions

$$\begin{aligned} \frac{1}{B} &> \pm\frac{f_{d2}}{k} + \frac{2v}{c}NT_p \\ v &< \frac{c}{2B\left(\frac{f_2}{k} + NT_p\right)} < \frac{c}{2B\left(\pm\frac{f_2}{k} + NT_p\right)} \end{aligned} \tag{24}$$

Above condition suggests that peak walking can be avoided by suitable setting system parameters. After that, we can make symbol decisions to get bit data in different channels, according to comparison between up-chirp and down-chirp on the magnitude of matching filter output at the symbol decision point, as shown at $t' = 0$ in Fig. 6. Finally, bit stream can be obtained through parallel to single module.

C. TARGET DETECTION MODULE

In consideration of loading communication information only on magnitude instead of phases, changes in signal's phase mirror the information on moving targets. Therefore, phase is extracted from each symbol to detect target, and block diagram of target detection module is shown as Fig. 7. Notice, in a single target scene or only for first-arrival path estimation, phases can be extracted from symbol decision points to moving target detection (MTD). But in multiple targets scene, it need utilize all samples in symbol to MTD.

In order to more clearly illustrate the relationship between phase and information on target, it is just to take a single target scene for example in this section. So we need only focus on phases of symbol decision point under the equation (24), and give the following two cases about phases according to equation (19).

Case 1: whether data is 1 or 0 for $S_{1\_base\_even}(0,\ 2n)$, the phase of its matching output can be expressed as

$$\begin{aligned} &s_{match\_up}(0, 2n) \\ &\approx \exp\left(j2\pi\frac{2v}{c}f_1 2nT_p\right)\exp\left[-j2\pi f_1 2nT_p\right] \\ &\quad\cdot \exp\left(-j2\pi f_1\frac{2R}{c}\right)\exp\left(j2\pi\frac{T_p}{2}f_d\right)\exp\left(-j\phi_0\right) \end{aligned} \tag{25}$$

Case 2: whether data is 1 or 0 for $S_{2\_base\_odd}(0,\ 2n+1)$, the phase of its matching output can be expressed as

$$\begin{aligned} &s_{match\_up}(0, 2n+1) \\ &\approx \exp\left[j2\pi\frac{2v}{c}f_2\left(2n+1\right)T_p\right] \\ &\quad\cdot \exp\left[-j2\pi f_2\left(2n+1\right)T_p\right]\exp\left(-j2\pi f_2\frac{2R}{c}\right) \\ &\quad\cdot \exp\left(j2\pi\frac{T_p}{2}f_{d2}\right)\exp\left(-j\phi_0\right) \end{aligned} \tag{26}$$

Afterward, MTD is used to matching filter outputs of even and odd symbols for estimation on doppler frequency

of targets, respectively. And results are given as below

$$\begin{aligned} S_{MTD\_even}(l) &= \sum_{n=0}^{N/2-1} s_{match}(0,2n)\exp\left(-j\frac{2\pi}{N/2}ln\right) \\ &= \frac{\sin\left[\pi\left(\frac{2v}{c}f_1T_pN - NT_pf_1 - l\right)\right]}{\sin\left[\frac{2\pi}{N}\left(\frac{2v}{c}f_1T_pN - NT_pf_1 - l\right)\right]} \\ &\quad \cdot \exp\left[j\frac{N-2}{N}\pi\left(\frac{2v}{c}f_1T_pN - NT_pf_1 - l\right)\right] \\ &\quad \cdot \exp\left(-j2\pi f_1\frac{2R}{c}\right)\exp\left[-j2\pi f_1T_p\right] \\ &\quad \times \exp\left(j\pi T_pf_d\right)\exp\left[-j\phi_0\right] \end{aligned} \tag{27}$$

$$\begin{aligned} S_{MTD\_odd}(l) &= \sum_{n=0}^{N/2-1} s_{match}(0,2n+1)\exp\left(-j\frac{2\pi}{N/2}ln\right) \\ &= \frac{\sin\left[\pi\left(\frac{2v}{c}f_2T_pN - NT_pf_2 - l\right)\right]}{\sin\left[\frac{2\pi}{N}\left(\frac{2v}{c}f_2T_pN - NT_pf_2 - l\right)\right]} \\ &\quad \cdot \exp\left[j\frac{N-2}{N}\pi\left(\frac{2v}{c}f_2T_pN - f_2T_pN - l\right)\right] \\ &\quad \cdot \exp\left(-j2\pi f_2\frac{2R}{c}\right)\exp\left(-j2\pi f_2T_p\right) \\ &\quad \times \exp\left(j3\pi f_{d2}T_p\right)\exp\left[-j\phi_0\right] \end{aligned} \tag{28}$$

where l is the index of doppler frequency points, and seen from the results of MTD processing, both of peaks for a target locate at $l_1 = 2vf_1T_pN/c - NT_pf_1$ and $l_2 = 2vf_2T_pN/c - NT_pf_2$ in both channels, respectively. It means that peaks need be paired under multiple targets environment. Of course, we also wish to make peak-pair locate at the same position for a common target. And then, considering the N -point periodicity of MTD, f_1T_p and f_2T_p can be set as integers by selection for f_1 and f_2 to remove NT_pf_1 and NT_pf_2 terms. Moreover, both frequency points located from doppler frequency $2vf_1T_pN/c$ and $2vf_2T_pN/c$ need be the same, meaning that the difference of frequency must be less than an half MTD resolution, so

$$\begin{aligned} \frac{2v}{c}(f_2 - f_1)T_pN &< \frac{1}{2} \\ v &< \frac{c}{4NT_pf_{shift}} \end{aligned} \tag{29}$$

If the limitation is met, the location at peaks can be expressed as

$$l_{reciever1} = \frac{2v}{c}f_2T_pN \approx \frac{2v}{c}f_1T_pN \tag{30}$$

After MTD, the value at peak can be given by

$$\begin{aligned} P_{even} &= \exp\left(-j2\pi f_1\frac{2R}{c}\right)\exp\left(j\pi T_pf_d\right) \\ &\quad \times \exp\left[-j2\pi f_1T_p\right]\exp\left(-j\phi_0\right) \end{aligned} \tag{31}$$

$$\begin{aligned} P_{odd} &= \exp\left(-j2\pi f_2\frac{2R}{c}\right)\exp\left(j3\pi T_pf_{d2}\right) \\ &\quad \times \exp\left(-j2\pi f_2T_p\right)\exp\left(-j\phi_0\right) \end{aligned} \tag{32}$$

So the difference on above phases can be get

$$\begin{aligned} P_{difference\_reciever1} &= \angle\left(P_{even}P^*_{odd}\right) \\ &= 2\pi f_{shift}\frac{2R}{c} - \pi T_p\frac{2v}{c}\left(2f_2 + f_{shift}\right) \\ &\quad + \mathrm{mod}\left(2\pi f_{shift}T_p, 2\pi\right) \end{aligned} \tag{33}$$

Finally, the equation (30) and (33) are simultaneously solved to get R and v. Notice that third term cannot be removed when $f_{shift}T_p$ is non-integer. And the phase at peak can be estimated by arctan function, the range of $P_{difference}$ is $[0, 2\pi)$, but that for arctan function is $(-\pi, \pi)$. Therefore, the phase acquired by arctan need be added 2π if it is negative, unless it will yield false results. Similarly, according to received signal model from equation (10), doppler peak and relationship between distance and phase for receiver 2 can be given as below

$$l_{reciever2} = \frac{v}{c}f_2T_pN \approx \frac{v}{c}f_1T_pN \tag{34}$$

$$\begin{aligned} P_{difference\_reciever2} &= \angle\left(P_{even}P^*_{odd}\right) \\ &= 2\pi f_{shift}\frac{R}{c} - \pi T_p\frac{v}{c}\left(2f_2 + f_{shift}\right) \\ &\quad + \mathrm{mod}\left(2\pi f_{shift}T_p, 2\pi\right) \end{aligned} \tag{35}$$

IV. SYSTEM PARAMETERS SETTING ON CFSK

According to requirement of desired maximum detection range R, velocity v and symbol transmission rate R_s, it is necessary to select system parameters appropriately, including T_p, N, f_1, f_2, f_{shift} and B. So we describe the relationship between system parameters and its performance in this section.

Considering the limitation of energy for a symbol with length T_p and the inverse relationship between R_s and T_p, so the range of transmission and detection is longer but R_s is lower along with increasing T_p. Besides, T_p need satisfy condition of $T_p > \tau_{\max} - \tau_{\min}$ in order to avoid inter-symbol interference.

According to equation (30), the velocity resolution and maximum unambiguous velocity can be obtained as follow

Velocity resolution:

$$\Delta v = \frac{c}{2f_2T_pN} \quad for\ reciever1 \tag{36}$$

$$\Delta v = \frac{c}{f_2T_pN} \quad for\ reciever2 \tag{37}$$

So velocity resolution is improved as N increasing but should not too large to avoid peak walking according to in equation (24) and equation (29).

Maximum unambiguous velocity:

$$v_{\max\_unambiguous} = \frac{c}{4f_2T_p} \quad for\ reciever1 \tag{38}$$

$$v_{\max\_unambiguous} = \frac{c}{2f_2T_p} \quad for\ reciever2 \tag{39}$$

Meanwhile, the maximum for velocity need consider together on equation (24), (29) and (36), and given as

TABLE 1. System design example I.

System Parameter	Symbol	Value
Chirp Bandwidth	B	10MHz
Symbol Period	T_p	5us
Carrier Frequency	f_0	20GHz
Frequency Offset	f_{shift}	200KHz
Number Of Symbols	N	600
Sampling Frequency	f_s	10MHz
Distance Of Target	R	660m
Velocity Of Target	v	20m/s

TABLE 2. System design Example II.

System Parameter	Symbol	Value
Chirp Bandwidth	B	10MHz
Symbol Period	T_p	5us
Carrier Frequency	f_0	20GHz
Frequency Offset	f_{shift}	66.67KHz
Number Of Symbols	N	600
Sampling Frequency	f_s	10MHz
Distance Of Target	$R_1 \ldots R_4$	390m,519m 780m,1020m
Velocity Of Target	$v_1 \ldots v_4$	7.5m/s,87.5m/s 747.5m/s,57.5m/s
Reflection Coefficient	$A_1 \ldots A_4$	1,0.8 0.6,0.4

follow.

$$v_{maximum} < min\left[\frac{c}{4f_2T_p}, \frac{c}{2B\left(\frac{f_2}{k}+NT_p\right)}\right] < \frac{c}{4NT_pf_{shift}} \quad for\ reciever1 \tag{40}$$

$$v_{maximum} < min\left[\frac{c}{2f_2T_p}, \frac{c}{B\left(\frac{f_2}{k}+NT_p\right)}\right] < \frac{c}{2NT_pf_{shift}} \quad for\ reciever2 \tag{41}$$

The accuracy of distance estimation:

It can be seen from equation (26) that phase at peak is determined jointly by distance and velocity of target, so the phase resolution a and velocity resolution Δv have influenced on the ranging accuracy ΔR.

Case 1: when the velocity of target is multiple of Δv, the real velocity can be obtained from output of MTD. So the ranging accuracy is

For receiver 1:

$$\begin{aligned} P_{difference}(R+\Delta R, v) - P_{difference}(R, v) &= a \\ 2\pi f_{shift}\frac{2\Delta R}{c} &= a \\ \Delta R &= \frac{ac}{4\pi f_{shift}} \end{aligned} \tag{42}$$

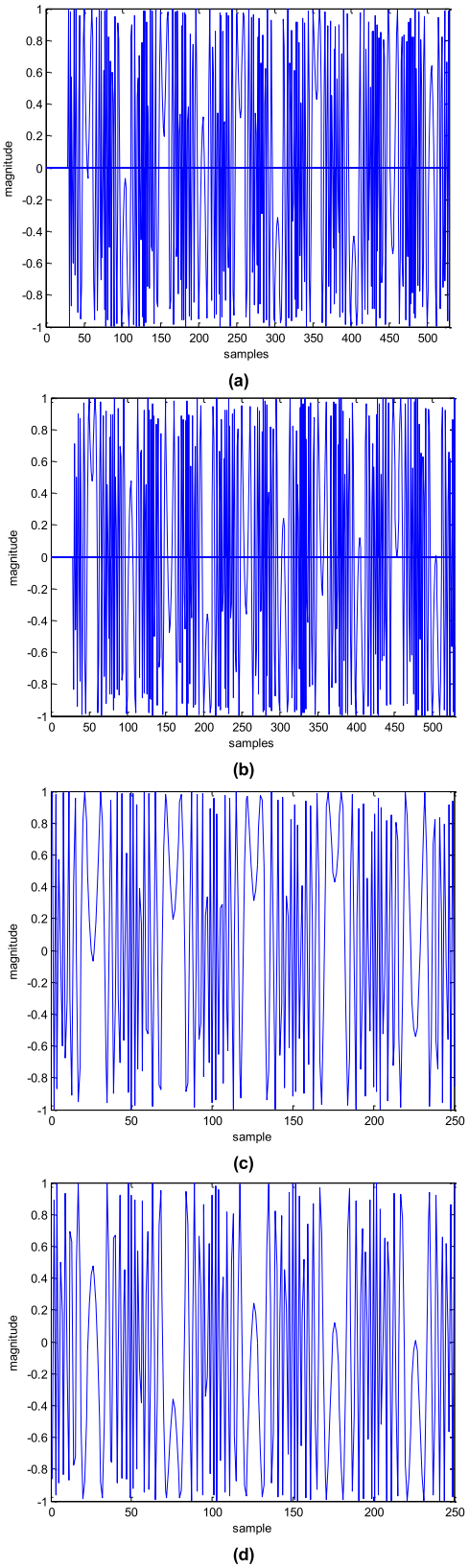

FIGURE 8. The baseband echo signal after mixers. (a) Baseband signal in channel 1. (b) Baseband signal in channel 2. (c) Odd symbols extracted from channel 1. (d) Even symbols extracted from channel 2.

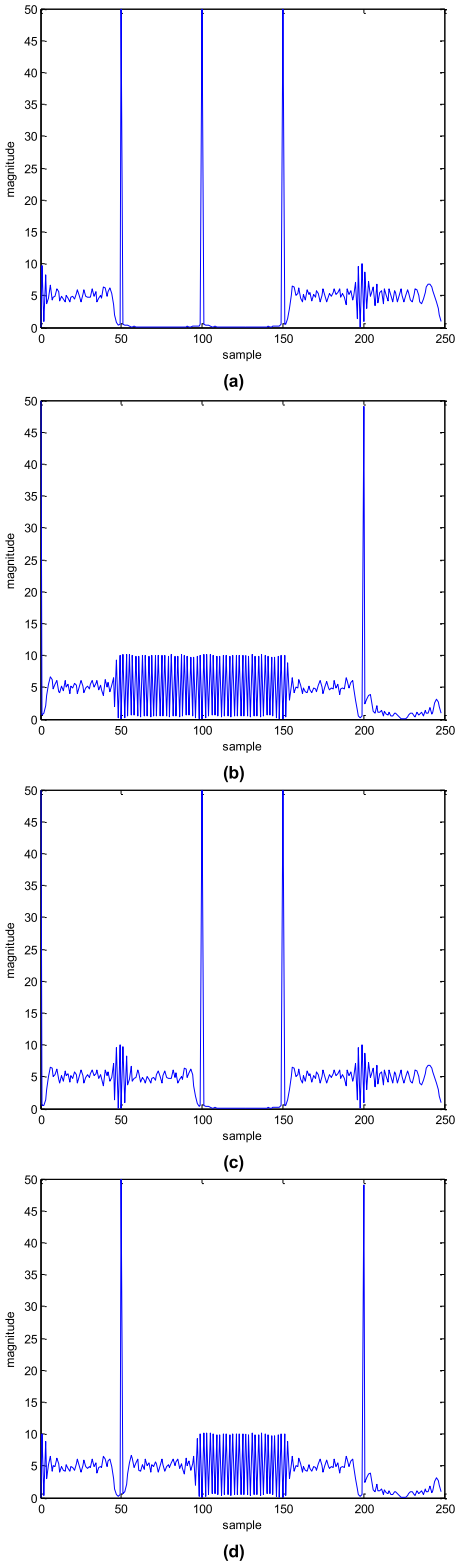

FIGURE 9. Matching output towards up-chirp and down-chirp in both channels. (a) Matching output towards up-chirp in channel 1. (b) Matching output towards down-chirp in channel 1. (c) Matching output towards up-chirp in channel 2. (d) Matching output towards down-chirp in channel 2.

For receiver 2:

$$\Delta R = \frac{ac}{2\pi f_{shift}} \tag{43}$$

Case 2: when the velocity of target is not multiple of Δv, the maximum velocity error is Δv towards output of MTD. So the distance accuracy is

$$\begin{aligned} &P_{difference}\left(R+\Delta R, v+\Delta v\right) - P_{difference}\left(R, v\right) = a \\ &2\pi f_{shift}\frac{2\Delta R}{c} - \pi T_p \frac{2\Delta v}{c}\left(2f_2 + f_{shift}\right) = a \\ &\Delta R = \frac{ac}{4\pi f_{shift}} + \frac{2\pi\,\Delta v T_p\left(2f_2 + f_{shift}\right)}{4\pi f_{shift}} \end{aligned} \tag{44}$$

So

$$\frac{ac}{4\pi f_{shift}} \le \Delta R \le \frac{ac}{4\pi f_{shift}} + \frac{\Delta v T_p\left(2f_2 + f_{shift}\right)}{2f_{shift}} \quad for\ reciever1$$

$$\frac{ac}{2\pi f_{shift}} \le \Delta R \le \frac{ac}{2\pi f_{shift}} + \frac{\Delta v T_p\left(2f_2 + f_{shift}\right)}{2f_{shift}} \quad for\ reciever2$$

Maximum unambiguous distance:

Due to 2π periodicity of phase from equation (33), its maximum unambiguous distance is limited as

For receiver 1

$$R_{unambiguous} \le \frac{c\left(2\pi - \mathrm{mod}\left(2\pi f_{shift} T_p, 2\pi\right)\right)}{4\pi f_{shift}} + \left(1 + \frac{f_2}{f_{shift}}\right) vT_p \tag{45}$$

For receiver 2

$$R_{unambiguous} \le \frac{c\left(2\pi - \mathrm{mod}\left(2\pi f_{shift} T_p, 2\pi\right)\right)}{2\pi f_{shift}} + \left(1 + \frac{f_2}{f_{shift}}\right) vT_p \tag{46}$$

Seen from above in equation, maximum unambiguous distance is determined mainly by f_{shift}. But f_{shift} impacts on the location of peak $S_{MTD\_\mathrm{odd}}(l)$ in equation (28), here f_{shift} is suggested to be a multiple of $1/NT_p$ so that peak walks integral units. With consideration of the relationship between f_{shift} and $R_{\max\_unambiguous}$, f_{shift} should be as small as possible, so the smallest one can be set as $1/NT_p$.

V. NUMERICAL EXAMPLES

In receiver 2, it just needs to utilize phases at symbol decision point to get information on distance and doppler of first arrival path or single target for receiver 2. On the contrary, it need utilize phases at all samples in each symbol for multi-target detection for receiver 1. Therefore, two simulations for the both receivers are given as below, and the parameters used in the simulation for receiver 2 and receiver 1 are listed in Table 1 and Table 2, respectively.

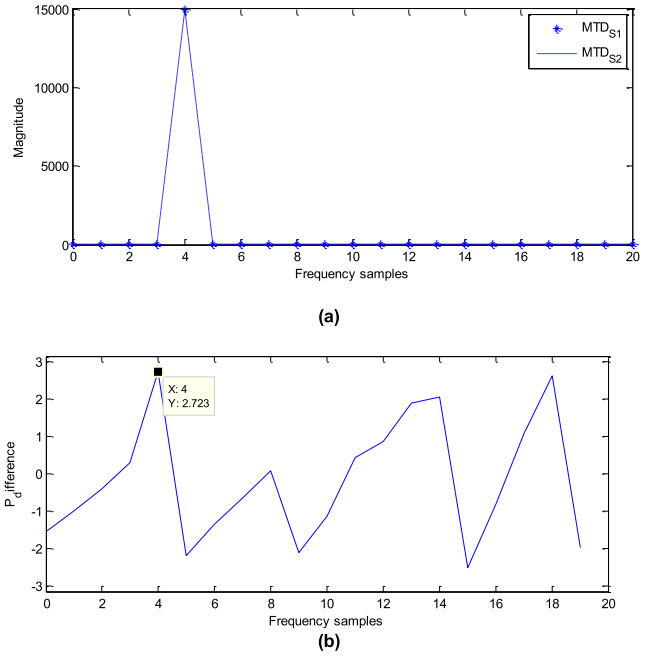

FIGURE 10. The output after MTD. (a) The output amplitude of MTD in both channels. (b) The difference on phases between both MTD.

A. THE SIMULATION FOR RECEIVER 2

Binary data for the previous ten symbols are assumed as follow

0	1	1	0	1	1	1	1	0	0

Then Baseband echo signal can be shown as Fig. 8.

After frame synchronization, the even and odd symbols are extracted from channel 1 and channel 2 respectively, shown as Fig.8 (c) and (d). And corresponding matching outputs are given as below.

Seen from Fig. 9, there is a clear difference on magnitude between outputs of matching and mismatching. After comparing amplitude, odd data can be get as shown in Fig. 9 (a) and (b), which is 0 1 1 1 0. And even data can be obtained as shown in Fig. 9 (c) and (d), which is 1 0 1 1 0. At last, we can get the original data after parallel to single.

Afterwards, MTD is processed to get target information in the both channels after matching filter, and outputs are shown as below.

Seen from the Fig. 10(a), the outputs amplitude of MTD in both channels are the same for a common target and its Doppler frequency locates at fourth frequency point. Considering velocity resolution for receiver 2 is $c/\left(NT_pf_0\right) = 5m/s$, the estimation of velocity should be 20m/s. The result is concordant with our hypothesis. But its probability of detection turns to be lower as velocity of target increases, the receiver

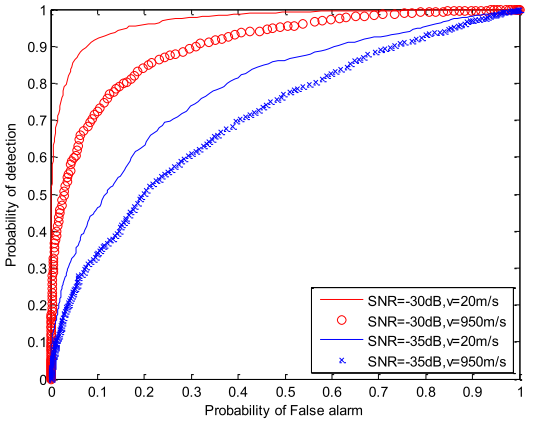

FIGURE 11. The receiver operating characteristic curve.

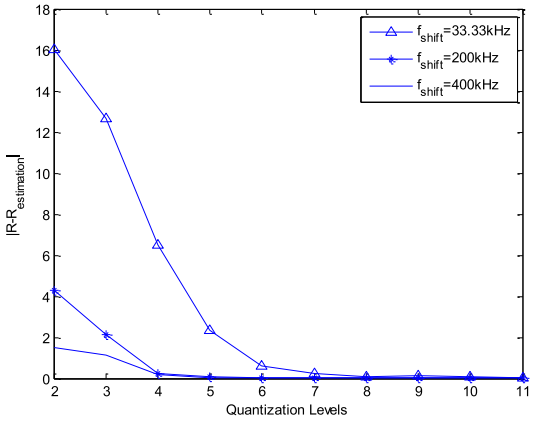

FIGURE 12. The relationship between ranging error and quantization levels.

operating characteristic curve (ROC) under various SNR and different velocity of target is shown as below.

Afterwards, the phase difference at peak is extracted from the outputs of both MTD, shown as marker in Fig. 10(b). According to above estimation of velocity and equation (35), the estimation of target distance R can be obtained, $R_{estimation}$, as shown at the bottom of this page.

It is enough to prove that equation (33) is reasonable in spite of that it exists a little error, which results from approximation of phases from equation (19). On the other hand, the ranging accuracy relies on the precision of phase acquired that depends from the quantization levels. The figure 12 gives a relationship between ranging error and quantization levels, it has converge to a small error when quantization level reaches 8. And it shows that ranging accuracy is inversely proportional to f_{shift} in accordance with equation (43).

Generally, the ADC's quantization levels, such as 14bit or 16bit, have been able to meet the requirement of high precision of phase. So the major problem focuses on the influence of noise on phase. For this, BER and detection

$$R_{estimation} = \frac{c\left[P_{difference\_reciever2} - \mathrm{mod}\left(2\pi f_{shift}T_p, 2\pi\right)\right] + \pi vT_p\left(2f_2 + f_{shift}\right)}{2\pi f_{shift}} \approx 660.068\mathrm{m}$$

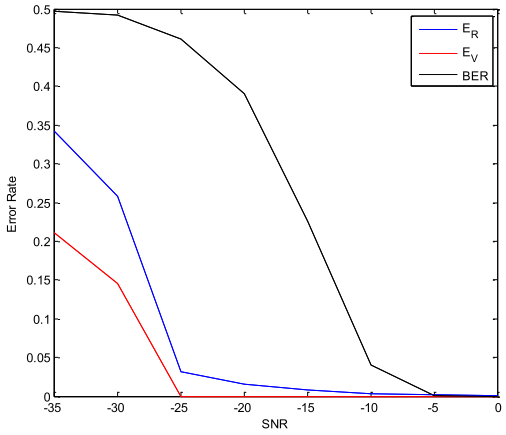

FIGURE 13. The results of BER and detection performance with Various SNR.

performance with Various SNR are shown as Fig. 13. In order to jointly evaluate the system performance, the normalized error of estimation towards distance and velocity are defined as

$$E_R = \frac{|R - R_{estimation}|}{R_{\max\_unambiguous}}$$
$$E_v = \frac{|v - v_{estimation}|}{v_{\max\_unambiguous}}$$

Seen from the Fig. 13, it indicates that this system can distance estimation under multi-target environment spectrum gain of Chirp. And since that coherent processing is used on target detection module, integration gain can be obtained for target detection. Therefore, the performance on target detection maintains good when SNR=−20dB in spite of that BER has been declined seriously.

B. THE SIMULATION FOR RECEIVER 1

Figure 13 gives results of MTD on all samples in symbol for multi-target detection. Notice that frequency offset $f_{shift} = 66.67kHz$ is no longer integral multiple of $1/T_p$, according to equation (27) and (28), position of targets in even symbol channel turn to be shift periodical by $f_{shift}NT_p = 200$ units along Y axis, as shown in Fig.14 (a) and (b). Of course, in order to make common target the same position in both channels, it should be shifted periodical by 200 units in reverse, as shown in Fig.14 (c). Furthermore, reference time point for target detection turns to be moment of frame synchronization instead of initial time of signal transmitted, means that the coordinate of first arrival target is 0 in relative distance axis and others are just relative value to first arrival target in distance axis. Table 3 lists estimation of distance and velocity for all targets. Compared to single target environment in simulation A, the accuracy of distance estimation under multi-target environment has declined a little, resulting from non-ideal sidelobes. But accuracy of distance estimation is still smaller traditional distance resolution $c/2B = 15m$, as seen from target 2. From target 3, it indicates that limitation of velocity can reach maximum of unambiguity velocity

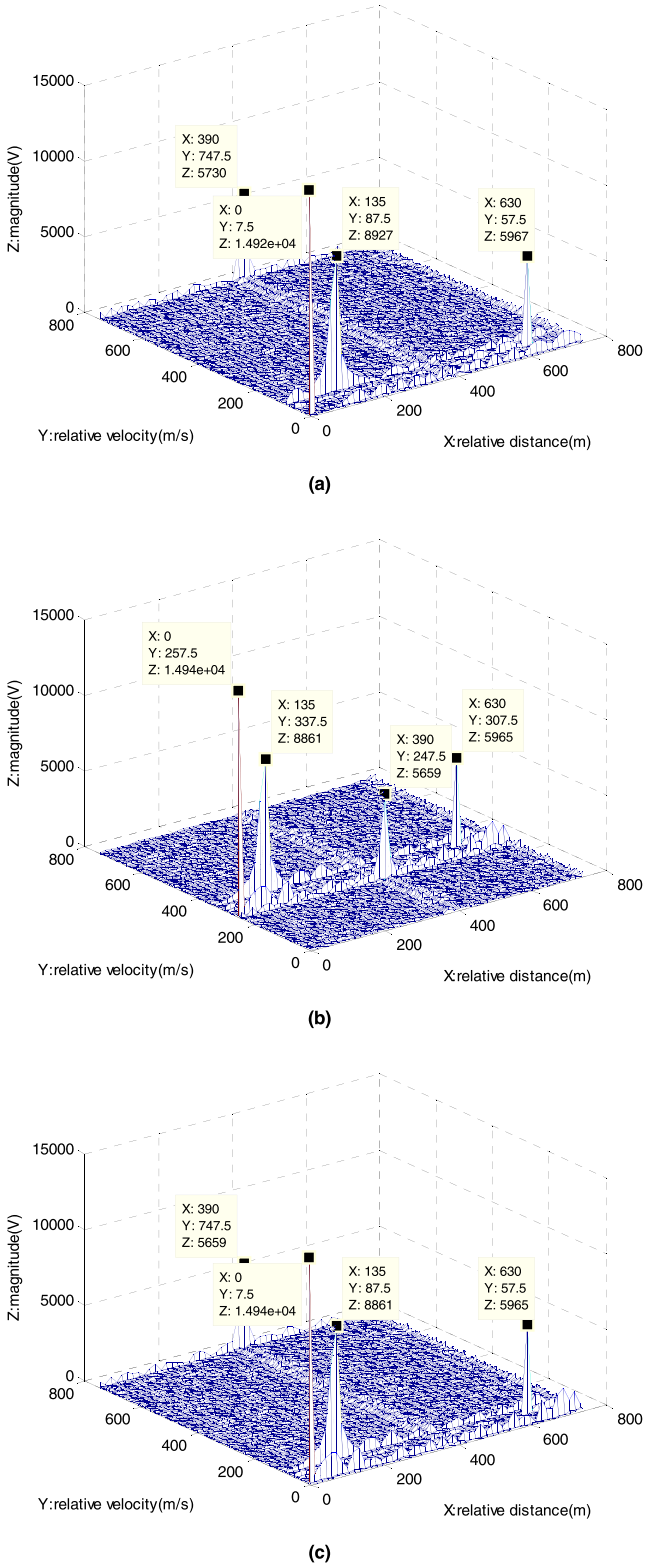

FIGURE 14. The results of MTD on all samples in symbol. (a) The output of MTD in odd symbol channel. (b) The output of MTD in even symbol channel. (c) The output of MTD after circular shift in even symbol channel.

in accordance with inequation (40). Besides, maximum of unambiguity distance is $cT_p/2 = 750m$ in traditional FMCW, but that in CFSK can be bigger, as seen from target 4.

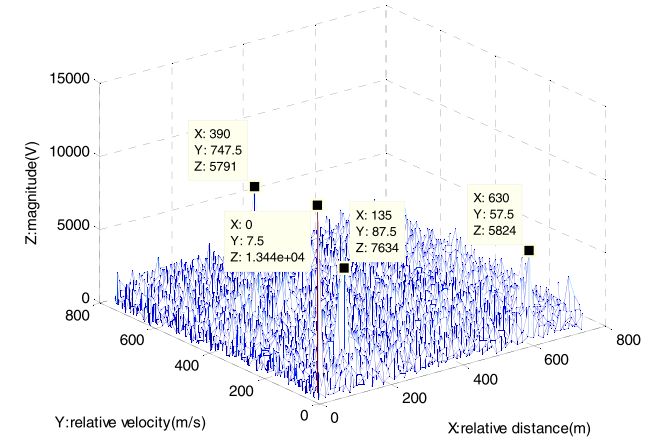

(a)

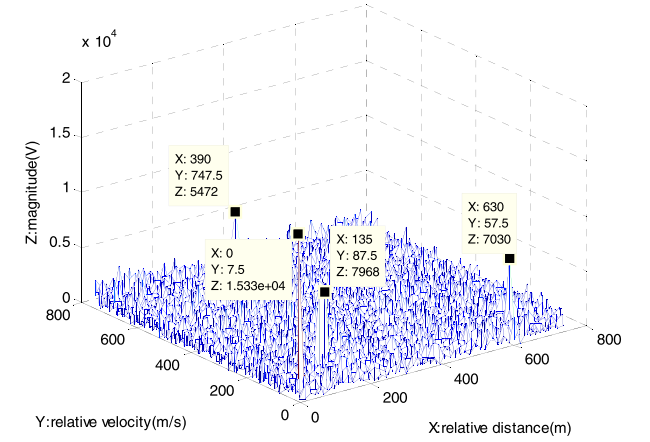

(b)

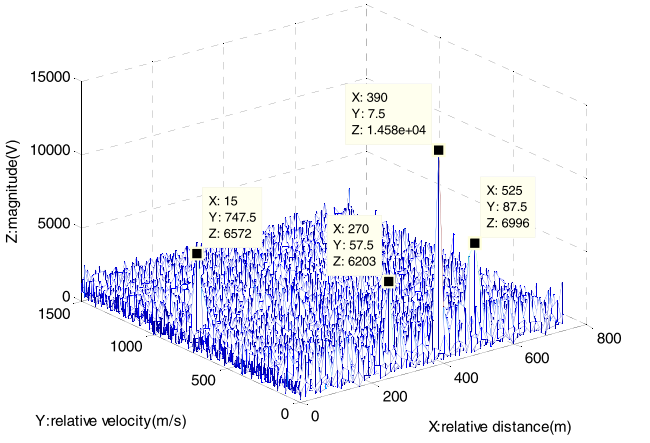

(c)

FIGURE 15. The results of MTD in SNR = −15. (a) The output of CFSK in odd symbol channel. (b) The output of CFSK after circular shift in even symbol channel. (c) The output of traditional FMCW.

However, distance estimation comes from phase information in CFSK so that it is sensitive to noise. Here, results in SNR = −15dB are shown as Fig.15.

From Table 4, it can be seen that distance unambiguity turns up for target 3 and target 4 in FMCW but not in CFSK.

TABLE 3. Multi-Target Distance and Velocity Estimation in CFSK (SNR = 0)

No noise	Target 1	Target 2	Target 3	Target 4
Target Coordinate	(0,7.5)	(135,87.5)	(390,747.5)	(630,57.5)
Target Velocity	7.5m/s	87.5m/s	747.5m/s	57.5m/s
Phase Difference	3.1575	3.1841	1.1490	4.7047
Distance Estimation	391.95m	521.48m	782.72m	1021.0m

TABLE 4. Multi-Target Distance and Velocity Estimation in CFSK and FMCW (SNR = −15)

SNR= -15	Target 1	Target 2	Target 3	Target 4
Target Velocity	7.5m/s	87.5m/s	747.5m/s	57.5m/s
Phase Difference	3.0374	3.1481	1.1446	4.2994
Distance Estimation CFSK	348.97m	508.59m	781.17m	875.86m
Distance Estimation FMCW	390m	525m	15m	57.5m

Nevertheless, noise is still a serious negative influence on distance estimation in CFSK compared with FMCW.

VI. CONCLUSION

The CFSK waveform combined between FSK and Chirp signal is presented for radar-communication integration, which can achieve both radar and communication function simultaneously in the same frequency bandwidth, and the derivation of algorithm on CFSK system for dual function is described in detail. In this method, matching filter method is used to process chirp whether it is applied in communication or radar, so that the complexity of the signal processing can be reduced, and impacts of doppler on matching output is considered. Finally, some parameter settings is analyzed for system performance, and it is validated by several simulations.

REFERENCES

[1] A. G. Stove, "Linear FMCW radar techniques," *Proc. Inst. Elect. Eng. F Radar Signal Process.*, vol. 10, no. 5, pp. 343–350, 1992.

[2] J.-Y. Yang, T.-B. Ling, and J. He, "MTD and range-velocity decoupling of LFMCW radar," *J. Electron. Inf. Technol.*, vol. 26, no. 2, pp. 169–173, 2004.

[3] Y. Fan, Z. Yang, X. Bu, and J. An, "Radar waveform design and multi-target detection in vehicular applications," in *Proc. IEEE Int. Conf. Estimation, Detection Inf. Fusion*, Jan. 2015, pp. 286–289.

[4] J. Park, H. Ryu, K.-W. Ha, J.-G. Kim, and D. Baek, "76–81-GHz CMOS transmitter with a phase-locked-loop-based multichirp modulator for automotive radar," *IEEE Trans. Microw. Theory Techn.*, vol. 63, no. 4, pp. 1399–1408, Apr. 2015.

[5] H. Rohling and M. M. Meinecke, "Waveform design principles for automotive radar systems," in *Proc. Int. Conf. Radar CIE*, Oct. 2001, pp. 1–4.

[6] M. Kronauge and H. Rohling, "New chirp sequence radar waveform," *IEEE Trans. Aerosp. Electron. Syst.*, vol. 50, no. 4, pp. 2870–2877, Oct. 2014.

[7] Y. K. Jeong and T.-K. Song, "Simultaneous multizone focusing method with orthogonal chirp signals," in *Proc. IEEE Ultrason. Symp.*, vol. 2, Oct. 2001, pp. 1517–1520.

[8] Y. Xie, R. Tao, and T. Wang, "Method of waveform design for radar and communication integrated system based on CSS," in *Proc. 1st Int. Conf. Instrum., Meas., Comput., Commun. Control*, Oct. 2011, pp. 737–739.
[9] C. Zhang and Q. Chen, "Design of signal-sharing for radar and communication," in *Proc. Int. Conf. Mechatronic Sci., Electr. Eng. Comput.*, Dec. 2013, pp. 1250–1253.
[10] X.-B. Li, R.-J. Yang, and W. Cheng, "Integrated radar and communication based on multicarrier frequency modulation chirp signal," *J. Electron. Inf. Technol.*, vol. 35, no. 2, pp. 406–412, 2013.
[11] P. Barrenechea, F. Elferink, and J. Janssen, "FMCW radar with broadband communication capability," in *Proc. IEEE Eur. Radar Conf. (EuRAD)*, Oct. 2007, pp. 130–133.
[12] W. Scheiblhofer, R. Feger, and A. Haderer, "Method to embed a datalink on FMCW chirps for communication between cooperative 77-GHz radar stations," in *Proc. IEEE Eur. Radar Conf. (EuRAD)*, Sep. 2015, pp. 181–184.
[13] M. A. Richards, *Fundamentals of Radar Signal Processing*. New York, NY, USA: McGraw-Hill, 2005.
[14] L. Teng, "Dopplet performance analysis of frequency stepped radar signal," *J. Mod. Radar*, vol. 18, no. 2, pp. 31–37, 1996.

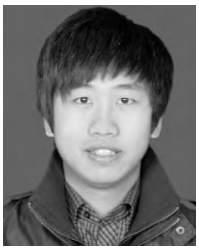

CHAO YANG was born in Xi'an, Shaanxi, China, in 1988. He received the M.S. degree in information and communication engineering from the Guilin University of Electronic Technology, Guilin, China, in 2015, where he is currently pursuing the Ph.D. degree. His research interests include broadband communication, clutter rejection, and radar communication integration.

MEI WANG received the M.S. and Ph.D. degrees in electronic engineering from Xidian University, Xi'an, China, in 1989 and 2003, respectively. She was with the Guangxi Wireless Broadband Communication and Signal Processing Key Laboratory, Guilin University of Electronic Technology. From 2006 to 2007, she was a Visiting Scholar with the University of Central Florida, Orlando. She is currently a Vice-Headmaster with the Guilin University of Technology. Her research interests are sensor networks, location awareness, and cooperative location.

LIN ZHENG was with the CDMA Department of ZTE, developing the CDMA2000 base station system from 2000 to 2003. After that, he began a doctorate program in UWB at Xidian University in 2003. He is also a Professor with the Guangxi Wireless Broadband Communication and Signal Processing Key Laboratory, Guilin University of Electronic Technology. His research interests are wireless sensor networks, wireless network clock synchronization technology, and wireless ultra-wideband communication and location.

CHAOCHEN TANG received the B.S. degree in electrical engineering from the Hebei University of Engineering, Hebei, China, and the M.S. degree in circuits and systems from Yanshan University, Hebei, in 2004 and 2008, respectively. He is currently pursuing the Ph.D. degree with Xidian University, Xi'an, China. In 2008, he joined the School of Information Science and Engineering, Guilin University of Technology, Guilin, China, as a Teaching Assistant, where he was subsequently promoted to a Lecturer. His research interests include radar communication integration, moving targets detection techniques, compressive sensing, and ISAR imaging.